SCIENTIFIC REPORTS

OPEN

SUBJECT AREAS:
MATERIALS CHEMISTRY
MATERIALS SCIENCE
PHYSICAL CHEMISTRY
NANOSCALE MATERIALS

Received
17 June 2013

Accepted
22 July 2013

Published
7 August 2013

Correspondence and requests for materials should be addressed to B.Y.G. (bygeng@mail.ahnu.edu.cn)

"Re-growth Etching" to Large-sized Porous Gold Nanostructures

Wenzheng Li, Long Kuai, Lu Chen & Baoyou Geng

College of Chemistry and Materials Science, The Key Laboratory of Functional Molecular Solids, Ministry of Education, Anhui Laboratory of Molecular-Based Materials, Anhui Normal University, Wuhu, 241000, P. R. China.

A new method, named "re-growth etching", which introduces a unique etchant "Au^{I}", has been developed to fabricate large-sized porous gold nanostructures. The size of nanostructures and the number of pores can be regulated by the molar ratio of Ag and Au in the precursor. We have evaluated their performance by a model reaction of the reduction of 4-nitrophenol. The catalytic property of porous Au from $Ag_{67.6}Au_{32.4}$ (Sample 3) is higher than those of other obtained products, which are mainly attributed to its hollows-interior, porous-exterior, and the large amount of Au. The method for the large-sized porous metal nanostructures has been established for the first time and shows the potential of this route to expand the scope of fabricating porous metal nanostructures.

Noble metal nanostructures with porous, hollow or frame structures have attracted great attention in several fields, such as catalysis[1–3], information storage[4], sensing[5], drug delivery[6], medical diagnostics[7] and biomedical imaging[7], because of their spatial configuration that displays low density, effective contact area and good fluid transmittance. In particular, many interesting issues of gold (Au) nanocrystals and/or clusters have been found and widely studied in the near two decades, for example, amazing catalytic performance[8], excellent and tunable plasmonic properties[9,10], photothermal therapy[11], and so forth. One of the most interesting cases of Au nanoparticles/clusters is the catalysis, which has been well reviewed by Gong et al.[12] It is known that the bulk Au possesses very poor catalytic performance because of the few readily adsorbed molecules in the surface. However, nanoscaled Au below 10 nm was founded to exhibit considerable performance, especially for the Au/metal oxides composite materials. Several researchers have developed splendid noble metal frameworks[13–15]. Porous noble metal nanostructures assembled with small nanoparticles blocks often exhibit outstanding performance due to their high specific surface area and large amount of metal content. Porous noble metal nanostructures including porous hollow nanoshells and non-hollow porous structures are usually fabricated, respectively, through galvanic replacement reactions with active metals as sacrificial templates and etching bimetallic nanostructures[1,16,17]. However, traditional etching route through a bimetallic precursor, such as Au/Ag, can only fabricate small-sized porous nanostructures. Protocol to fabricate large-sized (>100 nm) porous noble metal nanostructures would not be possible due to collapse or deformation in the process of growth. Unfortunately, small-sized porous nanostructures always suffer from the congregation during their application. Thus, fabrication of large-sized porous noble metal nanostructures is potentially very significant but still remains a challenge.

Herein, we develop a promising strategy named "re-growth etching" to fabricate large-sized porous Au nanostructures at room temperature with controlled size and pore number. In this case, Ag-Au bimetal nanostructures are used as precursors and Au^{I} as etchant. Galvanic replacement and Kirkendall effect are combined to play a vital role for the formation of large-sized porous Au during re-growth etching processes[18–20]. Compared with Au^{III}, Au^{I} has more oxidizing capacity and can avoid the unwanted reaction between Au^{III} and Au nanoparticles. Meanwhile, it is important to realize overgrowth by Au^{I} so that the size get larger than the unetched ones. With the well-defined morphology, the size of porous Au nanostructures can be controlled by adjusting the atomic percent in the bimetal precursor. Due to a principle that states structure determines properties, researching on framework of Au has been done by pioneer[1], and unique porous structures with large-sizes have enabled us to optimize the properties. Reducing 4-nitrophenol (4-NP) has been employed as a model catalysis study to demonstrate the potential for wider applications. The catalytic property of porous Au is higher than that of other obtained products, which is mainly attributed to its hollows-interior, porous-exterior, and the large amount of Au.

Results

Based on their close lattice constant, Xie et al have balanced the nucleation/growth speed of Ag and Au and synthesized Ag-Au alloy by co-reduction process[21]. Recently, we have also fabricated Ag-Au bimetal

nanostructures with controlled Ag/Au molar ratio through co-reduction route[22]. The morphology and size of the as-prepared nanoparticles were exhibited by SEM images in Figure S1a–c. The nanoparticle size can be adjusted directly by controlling the amount of Ag in bimetal which is fulfilled in the theoretical description of synthesis. The chemical composition about atomic percent of Ag and Au was indicated by energy dispersive X-ray (EDX) spectra (shown in Figure S1d–f) and ICP. Moreover, estimated from Figure S1a, b and Figure 1a, the average sizes of a signal nanoparticle are approximately 230 nm for $Au_{90.4}Au_{9.6}$, 225 nm for $Au_{83.3}Au_{16.7}$ and 180 nm for $Au_{67.6}Au_{32.4}$ (Figure S2c), respectively. Furthermore, a TEM image of $Ag_{67.6}Au_{32.4}$ is shown in Figure 1b with an average size of around 180 nm, along with the accompanying selected area electron diffraction (SAED) pattern inserted. High-resolution TEM image (Figure 1c) shows that the selected region of nanoparticle are highly crystalline with lattice fringes calculated to be 0.24 nm which is conformity to {111} planes of face-centered cubic Ag or Au. In addition, as shown in Figure 1d–g, high-angle annular dark-filed (HAADF) scanning transmission-electron microscopy (STEM) imaging and the EDX elemental mapping were used to study the elemental distribution of $Ag_{67.6}Au_{32.4}$. Obviously, the wide distribution of the elements of Ag and Au further confirmed the formation of bimetals.

Discussion

Removing Ag from Ag-Au alloy has been investigated previously. Generally, nitric acid, ferric nitrate, ammonia and other oxidation etchants[21,23–25] were selected to etch Ag-Au bimetals and cause the formation of hollow/porous nanostructures. But those selections have a common character that the used Ag-Au bimetals which were either alloy nanoboxes or nanotubes have empty layer instead of solid core before entirely removing Ag. Herein, we obtained the solid Ag-Au bimetal, in which a small amount of Au was accompanied with Ag coexisted in the whole nanostructures. As a consequence, it is difficult to obtain porous Au if an etchant will be used, and the entirely remaining nanostructures tend to collapse after etching because of less Au in the structures. A promising strategy is using $HAuCl_4$ as oxidation etchant via galvanic displacement which induces element Au production and finally increases the content of Au in the product. However, using the higher oxidation states of Au^{III} as etchant, the following chemical reactions of equations 1 and 2 could occur simultaneously.

$$3Ag + Au^{III} = 3Ag^{+} + Au \quad (1)$$

$$2Au + Au^{III} = 3Au^{I} \quad (2)$$

$$Ag + Au^{I} = Ag^{+} + Au \quad (3)$$

So, the control of the expectant nanostructures should be very difficult. Fortunately, different Au oxidation states possess different electrode potentials. Equation 4 and 5 shows the corresponding half electrode reactions of Au^{I} and Au^{III}, respectively.

$$AuCl_2^{-} + e = Au + 2Cl^{-}, \varphi^{\theta} = 1.15V \quad (4)$$

$$AuCl_4^{-} + 3e = Au + 4Cl^{-}, \varphi^{\theta} = 1.00V \quad (5)$$

Thus, to prevent the occurrence of equation 1 and 2, the strategy of introducing Au^{I} that also could remove Ag from bimetal shows extraordinary effect. And, it has amply proved that Au^{I} own the lower valence but higher oxidizing property than that of Au^{III}. As a result, we developed an alternative way to approach the original subject. The lower oxidation of Au^{I} instead of Au^{III} could avoid the occurrence of the equation 2. On the other hand, the stronger oxidizing capacity of Au^{I} would be more favorable for etching reaction and complete removal of Ag from bimetallic nanoparticles only with the equation 3.

The formation scheme of the porous Au is shown in Figure 2a. As soon as the Au^{I} solution is exposed to Ag-Au bimetal, the reaction of equation 3 was triggered. When galvanic replacement happened on the surface of Ag-Au bimetal where Ag is oxidized and electrons were stripped, Au^{I} captured electrons; then nuclear and growth of Au atoms occurred on the surface of bimetallic nanostructures. Cavities appeared and the dissolution of Ag^{+} increased the concentrations of Cl^{-} on locations of the etched Ag so that the pit grew by autocatalytic processes[26]. The formed AgCl is removed by using NH_4OH during washing products. When the initial Ag is etched from bimetals by Au^{I}, the dominant chemical potential difference between Au^{I} and Ag^{0} drives the occurrence of galvanic replacement reaction. Owning to the nanosacled Kirkendall effect[19], external vacancies diffuse inward until get boundary sites and voids become larger than initial status while the concentration of vacancy gradually increase[26]. Similar case was also found and well discussed in Zeng' work[27]. During the diffusion of vacancies, Au and Ag atoms diffuse outward (the diffusion rate of Au atoms slower than that of Ag atoms in Ag-Au bimetal[28]), and retained the cavities until pores are formed.

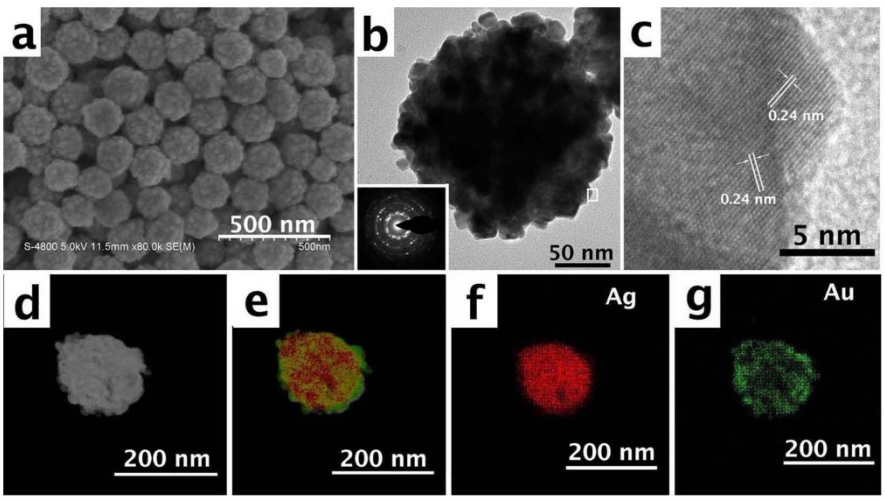

Figure 1 | SEM image (a) and TEM image (b) of $Ag_{67.6}Au_{32.4}$ nanoparticles, the corresponding SAED pattern inserted, (c) HRTEM image of the region in (b), (d) HAADF-STEM of one $Ag_{67.6}Au_{32.4}$ bimetallic nanoparticle, (e) Overlapped mapping image, and EDX elemental mappings of Ag (f) and Au (g).

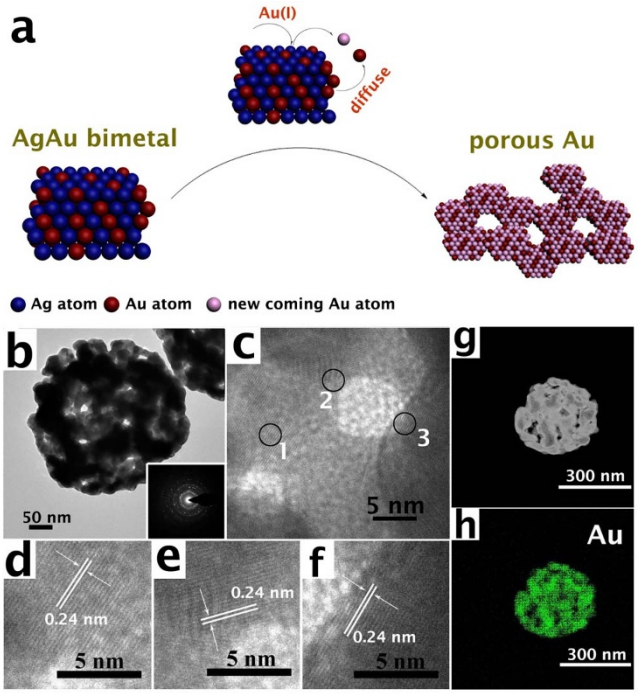

Figure 2 | (a) Schematic illustration of porous Au derived from Ag-Au bimetal via using Au (I) as etchant. (b) Sample 3 with very significant pores, the inset is the corresponding SEAD pattern. (c) HRTEM image of Sample 3. (d)–(f) the corresponding lattice-resolved TEM images from the regions 1, 2, and 3 in c. (g) HAADF-STEM image of porous Au and (h) EDX elemental mapping of Au.

The new Au atoms continue epitaxial growth with destroyed pores and resulting in the fabrication of large-sized Au nanostructures with hollow-interior and pore-exterior.

Figure S3a, b and c show the SEM images of Sample 1, 2 and 3 after etching $Ag_{90.4}Au_{9.6}$, $Ag_{83.3}Au_{16.7}$ and $Ag_{67.6}Au_{32.4}$, respectively. SEM images in Figure S3 reveal that many pores exist obviously on the surfaces of products, and void should also be ensured in every individual. The size-distribution of the products are shown in Figure S3d. Similar to other galvanic displacement between Ag and Au^{III}, the sizes of these products are clearly larger than the primary bimetals[1,22]. When the Au^{I} solution was added into the bimetal solution, reaction occurred immediately. In this case, Ag used as the sacrificed template and the new coming Au would grow on the original Au in Ag-Au bimetal. To ensure the reaction proceeds entirely, the amount of Au^{I} solution should be adjusted according to the precursors. When reactions ended, the new coming Au grown on the samples surfaces made the size enlarge markedly. The maximal size could reach about 500 nm from the precursor of $Ag_{90.4}Au_{9.6}$, and the minimal one about 300 nm from $Ag_{67.6}Au_{32.4}$. Significantly, without any residual Ag were found in the products from EDX results (Figure S4). TEM images (Figure S5a, 5b and Figure 2b) further demonstrate that hollow and porous Au nanostructures with large size are obtained. They have spherical morphology with an average size of around 300, 400 and 500 nm for Sample 1, 2 and 3, respectively. More pores emerged while little Ag existed in the bimetals and the average pore sizes are about 50 nm for Sample 1, 16 nm for Sample 2 and 11 nm for Sample 3. It provides that the comparatively smaller-size one (Sample 3) has more and smaller pores than the others. Moreover, SAED pattern (inserted in Figure 2b) for Sample 3 confirm polycrystalline feature of porous Au. HRTEM micrographs of regions 1, 2 and 3 (Figure 2c) and the lattice fringes of 0.24 nm (Figure 2d–f) are corresponded to the {111} planes of face-centered cubic Au. HAADF-STEM imaging and the EDX elemental mapping (Figure 2g and h) represent the elemental distribution of porous Au (Sample 3), which vividly demonstrates that the etching is thorough and the final products only contain element Au.

In addition, NH_4OH and $Fe(NO_3)_3$ aqueous solutions could also be used to dissolve the Ag from Au/Ag bimetallic nanostructures[21]. $Fe(NO_3)_3$ can etch Ag according to the equation of $Ag(s) + Fe(NO_3)_3(aq) = AgNO_3(aq) + Fe(NO_3)_2(aq)$; whereas, the dissolution of Ag with concentrated NH_4OH solution in the presence of oxygen is due to the formation of a water-soluble complex $[Ag(NH_3)_2]^+$. In the present work, we also attempted to promote reactions using such two etchants. Although NH_4OH and $Fe(NO_3)_3$ aqueous solutions was ever used to form Au monometallic nanostructures by etching Au/Ag nanoboxes and nanowires, we could not get a resemblance which not only get porous nanostructures but also entirely remove the Ag. As shown in Figure S6a, the collapsed nanostructures are clearly obtained by using strong oxidative Fe^{3+}. The EDX spectrum in Figure S6b directly illustrates that there is residual Ag in the etched nanostructures and the reaction between Fe^{3+} and Au has occurred which illustrated by using controlled trials as shown in UV-vis spectrum (Figure S6c). The results (SEM and EDX in Figure S7) after etching with NH_4OH was not as same as Au^{I}, even unlike $Fe(NO_3)_3$. The above results further illustrate that Au^{I} is an effective etchant to form large-sized porous Au nanostructures from bimetallic precursors through "re-growth etching" route. In addition, the synthesis of porous Au can be well controlled and reproduced easily.

Herein, we selected a model reaction of catalytic reduction of 4-nitrophenol (4-NP) to 4-aminophenol (4-AP) to evaluate the catalytic properties of these products. Usually, the reduction reaction of 4-NP could not occur even in two days' time with large excess of $NaBH_4$ as reductant without catalyt.[1] Figure 3 shows UV-vis spectra and the linear relations of $\ln[C(t)/C(0)]$ versus t as a topical reduction process by adding the Sample 3 as catalyst. The color of solution

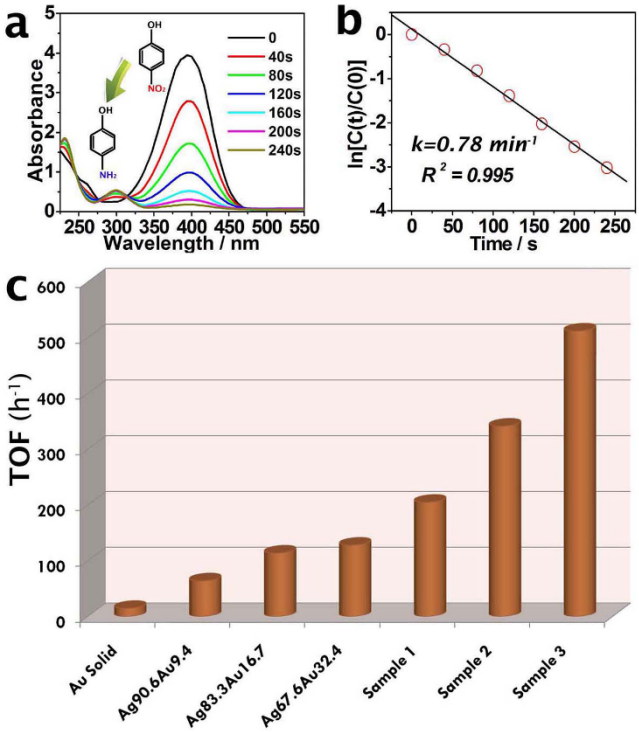

Figure 3 | (a) UV-vis spectra as a function of time catalyzed by Sample 3, indicating the disappearance of the absorbance for 4-NP due to the reduction of 4-NP into 4-AP. (b) Plot of $\ln[C(t)/C(0)]$ versus time for Sample 3. (c) The cylinder showing the analysis of TOF obtained from the results of reducing 4-NP by employing different catalysts.

changed from bright-yellow to the colorless in 4 min, indicating that 4-NP was entirely converted into 4-AP. For comparison, different Au-based nanostructures were collectively investigated as catalysts to reduce 4-NP. For all experiments, the concentrations of catalysts (1 mM), 4-NP (0.7 mM) and $NaBH_4$ (0.5 M) remain constant. Before catalysis, we know the content of Au in Ag-Au bimetals is different, the same number of particles we used in catalysis but the content of Au in $Ag_{67.6}Au_{32.4}$ is higher than the other two bimetals. After etching, Sample 1, 2 and 3 have the same content of Au, but the porous-exterior shown in the Figure 2b indicates Sample 3 probably have preponderance. The systematic results confirm the above speculation. UV-vis spectra of 4-NP reduction can be found in the supporting information (Figure S8a–f). The concentration of C(0) and C(t) is the corresponding concentration of 4-NP at the initiation and time t, which are gotten from the peak absorbance intensities of 4-NP in the UV-vis spectra. According to the physical chemistry principles, the linear relations of ln[C(t)/C(0)] versus t in Figure S8g–i showed that all of catalytic reduction reactions followed first-order kinetics. Moreover, the rate constants for first-order kinetic were also manifested by using plots of linear relationship. Table S1 shows experiment results using different samples for 4-NP catalytic reduction reactions. With the increasing of Au, the catalytic activity was enhanced (rate constants: 0.098 min^{-1}, 0.161 min^{-1} and 0.211 min^{-1} for $Ag_{90.6}Au_{9.4}$, $Ag_{83.3}Au_{16.7}$ and $Ag_{67.6}Au_{32.4}$, respectively).

Surprisingly, a great advance was made by our novel approach with Au^I as etchant, the catalytic efficiency of porous Au nanostructures was approximately 4 times than those of the original bimetals (rate constants: 0.306 min^{-1}, 0.592 min^{-1} and 0.78 min^{-1} for Sample 1, 2 and 3, respectively). Moreover, the catalytic activity of Sample 3 is over 45 times than solid Au nanoparticles (rate constant: 0.017 min^{-1}). Meanwhile, the actual product yields signify the catalytic activity, and TOF values could directly be connected with the quantitative analysis of the catalytic ability observed for different catalysts. Considering the size and number of the pore, they associated with each TOF values shown in Table S1 and the cylinder obviously represented the contrasted results which have been displayed in Figure 3c. For reducing 4-NP, Sample 3 as catalyst shown a highest TOF value of 511.9 h^{-1}, while the values of 14.6 h^{-1}, 64 h^{-1}, 113.8 h^{-1}, 128 h^{-1}, 204.8 h^{-1}, and 341.3 h^{-1} were observed for Au solid, $Ag_{90.6}Au_{9.4}$, $Ag_{83.3}Au_{16.7}$, $Ag_{67.6}Au_{32.4}$, Sample 1 and Sample 2, respectively.

Porous structures enhanced the function of diffusion in its apertures[14]: 1) providing paths to shorten the circle of diffusion; 2) by galvanic replacement and Kirkendall effect, there are many defects, vacancies and boundaries appeared with epitaxial growth; 3) the different pressure between interior and exterior would accelerate diffusion[29–31]; 4) in physics, a conventional macroscopic theory of "capillarity" usually emerges in pores[32]; the smaller is the pores, the more manifest will the capillarity be. However, perhaps, pores clogged when both reactants and products were passing the same paths and fluid transmittance was affected by this situation. So, the size of pore bellow 10 nm was not considered entirely.

In conclusion, we have developed a promising strategy of "re-growth etching" to fabricate large-sized porous Au nanostructures. By galvanic replacement and Kirkendall effect, this method has been enabling us to get different large-sized porous Au. This research would give a guide on the fabrication of lager-sized porous materials. However, for different materials, the etchant should be skilled selected during this case. Size and feature of pore can be regulated in a certain extent, which greatly relates to the amount of Au in the precursor. The results also demonstrated that these porous Au nanostructures displayed excellent catalytic activity using the model reaction of reducing 4-NP. This work clearly illustrates that, "re-growth etching" is an effective route to acquire large-sized porous nanostructure. Such porous nanostructures might possess widespread potential application in catalysis, sensor, disease detection and therapy, bioencapsulation and nanoelectronics.

Methods

Chemicals. All chemical reagents were used as received without further purification.

Synthesis of Ag-Au bimetallic nanoparticles. Ag-Au bimetals NPs were prepared by reducing $AgNO_3$ and $HAuCl_4$ using PVP (polyvinylpyrolidone) and ascorbic acid. In typical synthesis, $AgNO_3$ aqueous solution (2 mM) and 0.4 g PVP were mixed in a 25 mL glass vial with 5 mL deionized water and stirred 10 min. After the solution became clear, 2 mL 2.8% $NH_3 \cdot H_2O$ aqueous solution was added into the above mixture and stirred 2 min. Next, a certain amount of 2 mM $HAuCl_4$ aqueous solution was injected into the above mixture ((Ag + Au)/mole = 3 imol) using a syringe. The mixture was stirred for 5 min, followed by adding 1 mL of aqueous ascorbic acid solution (0.1 M). The clearly solution quickly reaction, after 15 min, reaction was stopped. Products were centrifuged with deionized water and ethanol several times at 8500 rpm to remove excess PVP, and then re-dispersed in 3 mL deionized water for the following use.

Synthesis of Au nanoparticle. 4 mL of 2 mM $HAuCl_4$ solution were used at the first step by adding PVP in aqueous solution, and the following steps were the same as the above mentioned, except the adding of $AgNO_3$. The products were washed and re-dispersed in deionized water for further use.

Synthesis of porous Au etched by Au^I. The Au^I solution was obtained by adding the appropriate volume of 1 mM AA solution to 1 mL 2 mM $HAuCl_4$ solution, upon which the yellow solution becomes colorless. 1 mL of the as-synthesized Ag-Au nanoparticles was mixed with a certain volume of $HAuCl_2$. The color of the mixture changed immediately when the Au^I solution was added. After the reaction process up to 2 h at room temperature, the resultant nanostructures were collected and washed with deionized water by centrifugation at 8000 rpm. The final product was dispersed in 1 mL deionized water.

Synthesis of porous Au etched by $Fe(NO_3)_3$. 1 mL of the as-synthesized Ag-Au nanoparticles was mixed with a certain volume of 20 mM $Fe(NO_3)_3$. The color of the mixture changed immediately when the $Fe(NO_3)_3$ solution was added. After the reaction process up to 30 min at room temperature, the resultant nanostructures were collected and washed with deionized water by centrifugation at 8000 rpm. The final product was dispersed in 1 mL deionized water.

Synthesis of porous Au etched by NH_3H_2O. 1 mL of the as-synthesized Ag-Au nanoparticles was mixed with 2 ml 3% NH_3H_2O. After the reaction process up to 12 h at room temperature, the resultant nanostructures were collected and washed with deionized water by centrifugation at 8000 rpm. The final product was dispersed in 1 mL deionized water.

Characterization. The samples were characterized by scanning electron microscopy (SEM) (Hitachi S-4800 Japan), energy-dispersive X-ray (EDX) spectrometry (Hitachi S-4800 Japan), and transmission electron microscopy (TEM) (Tecnai 20S-TWIN Holland). UV-visible extinction spectra were recorded at room temperature by using U4100 at 220 V 50 Hz (Hitachi, Japan). The elemental distributions are performed by using a JEM-2100F (JEOL, Japan) equipped with energy dispersive spectrometer (EDX) analysis.

Catalytic reduction of 4-nitrophenol. In the typical process, 1 mL 0.7 mM 4-nitrophenol was mixed with 1 mL 0.5 M $NaBH_4$ (freshly prepared). Then, 20 iL Au-based nanocatalyst was injected into the system. The volume of the whole mixture solution was kept in 3 mL. Next, the mixed solution was quickly taken into a quartz cuvette to continuously measure the extinction spectra until the yellow solution became colorless.

1. Zeng, J., Zhang, Q., Chen, J. Y. & Xia, Y. N. A Comparison Study of the Catalytic Properties of Au-Based Nanocages, Nanoboxes, and Nanoparticles. *Nano Lett.* **10**, 30–35 (2010).
2. Zhang, H. *et al.* Facile Synthesis of Pd-Pt Alloy Nanocages and Their Enhanced Performance for Preferential Oxidation of CO in Excess Hydrogen. *ACS Nano* **5**, 8212–8222 (2011).
3. Cui, C. H. *et al.* Remarkable Enhancement of Electrocatalytic Activity by Tuning the Interface of Pd-Au Bimetallic Nanoparticle Tubes. *ACS Nano* **5**, 4211–4218 (2011).
4. Zeng, J. *et al.* Necklace-like Noble-Metal Hollow Nanoparticle Chains: Synthesis and Tunable Optical Properties. *Adv. Mater.* **19**, 2172–2176 (2007).
5. Xu, C. X., Liu, Y. Q., Su, F., Liu, A. H. & Qiu, H. J. Nanoporous PtAg and PtCu alloys with hollow ligaments for enhanced electrocatalysis and glucose biosensing. *Biosens. Bioelectron.* **27**, 160–166 (2011).
6. Yolanda, V., Amandeep, K. S. & Raymond, E. S. One-Pot Synthesis of Hollow Superparamagnetic CoPt Nanospheres. *J. Am. Chem. Soc.* **127**, 12504–12505 (2005).

7. Tartaj, P., Morales, M. P., Veintemillas-Verdaguer, S., González-Carreño, T. & Serna, C. J. The preparation of magnetic nanoparticles for applications in biomedicine. *J. Phys. D: Appl. Phys.* **36**, R182–R197 (2003).
8. Haruta, M., Yamada, N., Kobayashi, T. & Lijima, S. Gold catalysts prepared by coprecipitation for low-temperature oxidation of hydrogen and of carbon monoxide. *J. Catal.* **115**, 301–309 (1989).
9. Chen, H. J., Shao, L., Li, Q. & Wang, J. F. Gold nanorods and their plasmonic properties. *Chem. Soc. Rev.* **42**, 2679–2724 (2013).
10. Gong, J. L. *et al.* Micro- and Nanopatterning of Inorganic and Polymeric Substrates by Indentation Lithography. *Nano Lett.* **10**, 2702–2708 (2010).
11. Fang, C. H. *et al.* A gold nanocrystal/poly(dimethylsiloxane) composite for plasmonic heating on microfluidic chips. *Adv. Mater.* **24**, 94–98 (2012).
12. Gong, J. L. Structure and Surface Chemistry of Gold-Based Model Catalysts. *Chem. Rev.* **112**, 2987–3054 (2012).
13. Chen, J. Y. *et al.* Gold Nanocages: Bioconjugation and Their Potential Use as Optical Imaging Contrast Agents. *Nano Lett.* **5**, 473–477 (2005).
14. Hong, X., Wang, D. S., Cai, S. F., Rong, H. P. & Li, Y. D. Syntheses of Water-Soluble Octahedral, Truncated Octahedral, and Cubic Pt–Ni Nanocrystals and Their Structure–Activity Study in Model Hydrogenation Reactions. *J. Am. Chem. Soc.* **134**, 18165–18168 (2012).
15. Xia, B. Y., Wu, H. B., Wang, X. & Lou (David), X. W. One-Pot Synthesis of Cubic $PtCu_3$ Nanocages with Enhanced Electrocatalytic Activity for the Methanol Oxidation Reaction. *J. Am. Chem. Soc.* **134**, 13934–13937 (2012).
16. Wang, S. Z. *et al.* A Highly Efficient, Clean-Surface, Porous Platinum Electrocatalyst and the Inhibition Effect of Surfactants on Catalytic Activity. *Chem. Eur. J.* **19**, 240–248 (2013).
17. Lu, Y. *et al.* Hydrophilic Co@Au Yolk/Shell Nanospheres: Synthesis, Assembly, and Application to Gene Delivery. *Adv. Mater.* **22**, 1407–1411 (2010).
18. Snyder, J., Asanithi, P., Dalton, A. B. & Erlebacher, J. Stabilized Nanoporous Metals by Dealloying Ternary Alloy Precursors. *Adv. Mater.* **20**, 4883–4886 (2008).
19. González, E., Arbiol, J. & Puntes, V. F. Carving at the Nanoscale: Sequential Galvanic Exchange and Kirkendall Growth at Room Temperature. *Science* **334**, 1377–1380 (2011).
20. Yin, Y. D. *et al.* Formation of Hollow Nanocrystals through the Nanoscale Kirkendall Effect. *Science* **304**, 711–714 (2004).
21. He, W. W. *et al.* Design of AgM Bimetallic Alloy Nanostructures (M = Au, Pd, Pt) with Tunable Morphology and Peroxidase-Like Activity. *Chem. Mater.* **22**, 2988–2994 (2010).
22. Li, W. Z., Kuai, L., Qing, Q. & Geng, B. Y. Ag–Au bimetallic nanostructures: co-reduction synthesis and their component-dependent performance for enzyme-free H_2O_2 sensing. *J. Mater. Chem. A* **1**, 7111–7117 (2013).
23. Lu, X. M. *et al.* Fabrication of Cubic Nanocages and Nanoframes by Dealloying Au/Ag Alloy Nanoboxes with an Aqueous Etchant Based on $Fe(NO_3)_3$ or NH_4OH. *Nano Lett.* **7**, 1764–1769 (2007).
24. Zhang, Q. *et al.* Dissolving Ag from Au–Ag alloy nanoboxes with H_2O_2: A method for both tailoring the optical properties and measuring the H_2O_2 concentration. *J. Phys. Chem. C* **114**, 6396–6400 (2010).
25. Mulvihill, M. J., Ling, X. Y., Henzie, J. & Yang, P. D. Anisotropic etching of silver nanoparticles for plasmonic structures capable of single-particle SERS. *J. Am. Chem. Soc.* **132**, 268–274 (2010).
26. McEachran, M. *et al.* Ultrathin gold nanoframes through surfactant-free templating of faceted pentagonal silver nanoparticles. *J. Am. Chem. Soc.* **133**, 8066–8069 (2011).
27. Zeng, H. B. *et al.* ZnO-Based Hollow Nanoparticles by Selective Etching: Elimination and Reconstruction of Metal-Semiconductor Interface, Improvement of Blue Emission and Photocatalysis. *ACS Nano* **2**, 1661–1670 (2008).
28. Yen, C. W., Mahmoud, M. A. & El-Sayed, M. A. Photocatalysis in Gold Nanocage Nanoreactors. *J. Phys. Chem. A* **113**, 4340–4345 (2009).
29. Zeng, H. B. *et al.* Blue Luminescence of ZnO Nanoparticles Based on Non-Equilibrium Processes: Defect Origins and Emission Controls. *Adv. Funct. Mater.* **20**. 561–572 (2010).
30. Sun, Y. G. & Xia, Y. N. Mechanistic Study on the Replacement Reaction between Silver Nanostructures and Chloroauric Acid in Aqueous Medium. *J. Am. Chem. Soc.* **126**, 3892–3901 (2004).
31. Shibata, T. *et al.* Size-Dependent Spontaneous Alloying of Au−Ag Nanoparticles. *J. Am. Chem. Soc.* **124**, 11989–11996 (2002).
32. Jayaraman, K. *et al.* Observing Capillarity in Hydrophobic Silica Nanotubes. *J. Am. Chem. Soc.* **127**, 17385–17392 (2005).

Acknowledgments

This work was supported by the National Natural Science Foundation of China (20671003, 20971003 and 21271009), the Key Project of Chinese Ministry of Education (209060), the Program for New Century Excellent Talents in University (NCET 11-0888), the Doctoral Fund of Ministry of Education of China (20123424110002), the Science and Technological Fund of Anhui Province for Outstanding Youth (10040606Y32, 1308085JGD01), the Foundation of Key Project of Natural Science of Anhui Education Committee (KJ2012A143) and the Program for Innovative Research Team at Anhui Normal University.

Author contributions

W.L. performed the experiments, collected and analyzed the data, and wrote the paper; L.K. & L.C. helped with data analysis; B.G. conceived the experiments, analyzed results, and wrote the paper. All authors reviewed the manuscript.

Additional information

Supplementary information accompanies this paper at http://www.nature.com/scientificreports

Competing financial interests: The authors declare no competing financial interests.

How to cite this article: Li, W.Z., Kuai, L., Chen, L. & Geng, B.Y. "Re-growth Etching" to Large-sized Porous Gold Nanostructures. *Sci. Rep.* **3**, 2377; DOI:10.1038/srep02377 (2013).